SAVE THE DATE

01 - 03, December
HNBK International Convention Center

ASGO 2023

TAIPEI www.asgo2023.org

The 8th Biennial Meeting of Asian Society of Gynecologic Oncology

JOURNAL OF
GYNECOLOGIC
ONCOLOGY

Original Article

Check for updates

Integrated analysis of DNA methylome and transcriptome reveals SFRP1 and LIPG as potential drivers of ovarian cancer metastasis

Jiani Yi [1,*] Mengting Wu [2,*] Zhihong Zheng [2] Qing Zhou [2] Xufan Li [1] Yan Lu [2,3] Pengyuan Liu [1,3]

[1]Key Laboratory of Precision Medicine in Diagnosis and Monitoring Research of Zhejiang Province, Sir Run Run Shaw Hospital and Institute of Translational Medicine, Zhejiang University School of Medicine, Hangzhou, China
[2]Zhejiang Provincial Key Laboratory of Precision Diagnosis and Therapy for Major Gynecological Diseases, Department of Gynecologic Oncology, Women's Hospital and Institute of Translational Medicine, Zhejiang University School of Medicine, Hangzhou, China
[3]Cancer Center, Zhejiang University, Hangzhou, China

OPEN ACCESS

Correspondence to
Pengyuan Liu
Institute for Translational Medicine, Zhejiang University School of Medicine, Hangzhou, Zhejiang 310029, China.
Email: pyliu@zju.edu.cn

*Jiani Yi and Mengting Wu contributed equally to this work.

ORCID iDs
Jiani Yi
https://orcid.org/0000-0003-1636-5736
Mengting Wu
https://orcid.org/0000-0003-1737-4327
Zhihong Zheng
https://orcid.org/0000-0003-0966-5968

ABSTRACT

Objective: More than 75% of ovarian cancer patients are diagnosed at advanced stages and die of tumor cell metastasis. This study aimed to identify new epigenetic and transcriptomic alterations associated with ovarian cancer metastasis.
Methods: Two cell sublines with low- and high-metastasis potentials were derived from the ovarian cancer cell line A2780. Genome-wide DNA methylome and transcriptome profiling were carried out in these two sublines by Reduced Representation Bisulfite Sequencing and RNA-seq technologies. Cell-based assays were conducted to support the clinical findings.
Results: There are distinct DNA methylation and gene expression patterns between the two cell sublines with low- and high-metastasis potentials. Integrated analysis identified 33 methylation-induced genes potentially involved in ovarian cancer metastasis. The DNA methylation patterns of two of them (i.e., SFRP1 and LIPG) were further validated in human specimens, indicating that they were hypermethylated and downregulated in peritoneal metastatic ovarian carcinoma compared to primary ovarian carcinoma. Patients with lower SFRP1 and LIPG expression tend to have a worse prognosis. Functionally, knockdown of SFRP1 and LIPG promoted cell growth and migration, whereas their overexpression resulted in the opposite effects. In particular, knockdown of SFRP1 could phosphorylate GSK3β and increase β-catenin expression, leading to deregulated activation of the Wnt/β-catenin signaling.
Conclusion: Many systemic and important epigenetic and transcriptomic alterations occur in the progression of ovarian cancer. In particular, epigenetic silencing of SFRP1 and LIPG is a potential driver event in ovarian cancer metastasis. They can be used as prognostic biomarkers and therapeutic targets for ovarian cancer patients.

Keywords: Ovarian Cancer; DNA Methylation; Tumor Suppressor Gene; RNA-Seq; Metastasis

Qing Zhou [iD]
https://orcid.org/0000-0003-0995-9800
Xufan Li [iD]
https://orcid.org/0000-0002-0775-3510
Yan Lu [iD]
https://orcid.org/0000-0002-5004-4656
Pengyuan Liu [iD]
https://orcid.org/0000-0002-8386-8416

Synopsis
Many systemic and important epigenetic and transcriptomic alterations have been detected in the progression of ovarian cancer. Among them, SFRP1 and LIPG function as tumor suppressors in ovarian cancer, and their epigenetic silencing is a potential driver event of ovarian cancer metastasis.

INTRODUCTION

Ovarian cancer is the second most common malignancy in women [1]. More than 75% of affected women are diagnosed at advanced stages with vague and mild symptoms. The five-year survival rate is less than 30% for women with advanced-stage tumors [2]. Most patients develop metastatic disease after surgery and chemotherapy. Hence, a major barrier to the treatment of ovarian cancer is to identify novel prognostic biomarkers that can distinguish patients at high risk for relapse and to determine whether these biomarkers are potential therapeutic targets.

DNA methylation is a major type of epigenetic modification [3,4] that can alter gene expression without change of the DNA sequences. It mainly occurs at the cytosine residue of cytosine-phosphate-guanine (CpG) dinucleotides in the genome. Aberrant promoter CpG methylation is a common event in the initiation and progression of cancer [5]. It leads to dysregulation of many important pathways in cancer, including inactivation of tumor suppressor, loss of cell cycle control, altered function of transcription factor, disruption of cell-cell junctions, genomic instability, metabolic rewiring, immunosuppressive tumor microenvironment, and others [6].

Previous studies have shown that DNA methylation plays an important role in ovarian carcinogenesis and progression [7,8]. Several tumor suppressor genes such as BRCA1 [9-11], RASSF1A [12], OPCML [13-15], and P16INK4a [16] have been shown to be heavily hypermethylated in their promoter regions in ovarian cancer. Such promoter hypermethylation also frequently occurs in the DNA regions that code for miRNAs such as miR-34a and miR-30, and transcription factors such as KLF11 and the PolyComb group targets in ovarian cancer [17,18]. Changes in DNA methylation are associated with cisplatin resistance [19] and histology [20] in ovarian cancer.

In this study, we performed single cell cloning of an ovarian cancer cell line (A2780) and established two cell sublines with low- and high-metastasis potentials (**Fig. 1**). To investigate the potential mechanisms underlying ovarian cancer metastasis, we analyzed genome-wide DNA methylation profiles using Reduced Representation Bisulfite Sequencing (RRBS) and transcriptome profiles using RNA Sequencing (RNA-seq) in these two newly established cell sublines [21]. By integrated analysis of DNA methylome and transcriptome profiles, we identified 33 genes with aberrant methylation that are potentially associated with ovarian cancer metastasis. DNA methylation patterns of two of them (i.e., SFRP1 and LIPG) were further validated in peritoneal metastatic ovarian carcinomas compared to primary ovarian carcinomas. Finally, we experimentally confirmed their tumor-suppressive roles in ovarian cancer cells, which depend on promoter hypermethylation.
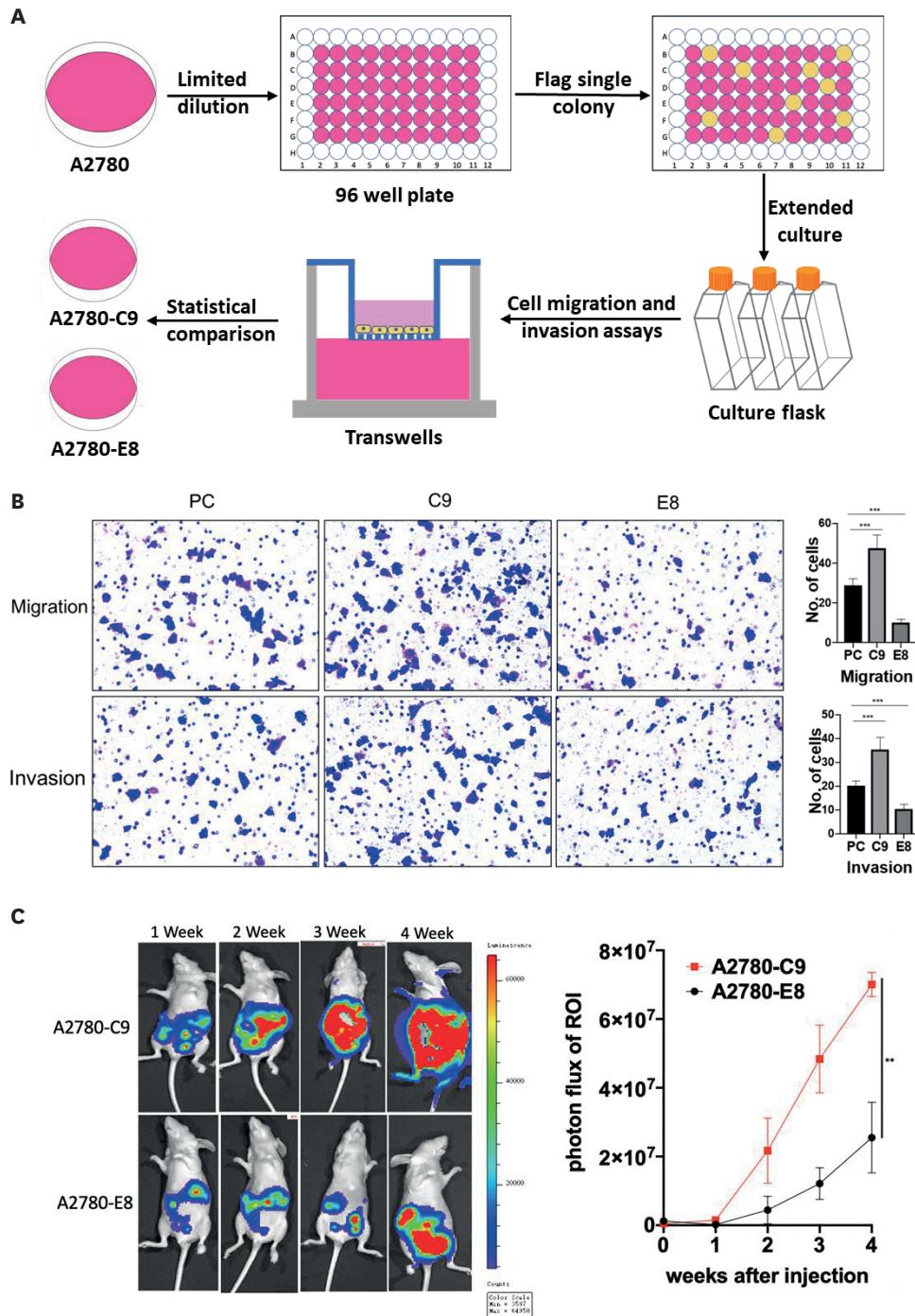
Fig. 1. Establishing ovarian cancer cell lines with low- and high-metastatic potential by single cell cloning. (A) A workflow for single-cell cloning of A2780. (B) In vitro migration and invasion abilities of A2780-WT, A2780-C9 and A2780-E8 measured in transwell assays at 24 hours. All good clones were evaluated for their metastatic potentials using transwell assays. A2780-C9 and A2780-E8 were identified as the sublines with the highest and lowest metastatic potentials, respectively. (C) In vivo invasion abilities of A2780-C9 and A2780-E8 measured in athymic nude mice. The A2780-C9 and A2780-E8 sublines were transfected with HBLV-LUC-BSD virus to obtain cells stably expressing firefly luciferase, and then injected intraperitoneally into nude mice. Data are presented as mean ± SD; n=3.
**p<0.01, ***p<0.001.

MATERIALS AND METHODS

1. Single cell cloning

Ovarian cancer cells of A2780 at log phase were collected and adjusted to a density of 10/mL with RPMI-1640 (Gibco, Carlsbad, CA, USA) and seeded into a 96-well plate (0.1 mL/well). The 96-well plate was observed under a microscope, and then a mark was made on the wells that contained a single cell. After being cultured for two to three weeks at 37°C and 5% CO_2 condition, good clones were selected and amplified for subsequent transwell assays.

2. Cell migration and invasion assays

The cells were cultured with serum-free RPMI 1640 medium for 24 hours, then detached and resuspended in serum-free RPMI 1640 medium. Cells were concentrated to $3×10^4$ cells in 300 uL cell suspension and then added to the upper transwell chamber (Corning Costar, Tewksbury, MA, USA) for the migration assay or the upper chamber coated with Matrigel for the invasion assay. The RPMI 1640 medium supplemented with 10% FBS was added to the bottom chamber. Cells that migrated into the bottom chamber were stained with 0.1% crystal violet. Images were captured from each membrane and the number of migratory cells was counted under a microscope.

3. Library preparation for methylation sequencing

Genomic DNA was extracted from cultured cells using PureLink Genomic DNA Mini Kits (Thermo Fisher Scientific, Waltham, MA, USA). DNA methylation sequencing analysis was performed in A2780-C9 and A2780-E8 sublines. Three biological replicates were done for each cell subline. Libraries for RRBS were generated according to protocols described by Gu et al. [21], followed by sequencing (per Illumina protocols) with modifications to allow multiplexing [22]. The libraries underwent cluster generation using TruSeq PE Cluster Kit v4-cBot-HS and paired-end sequencing using TruSeq SBS Kit v4-HS (Illumina, San Diego, CA, USA). RRBS libraries were multiplexed and sequenced on an Illumina HiSeq 2500 sequencer (**Table S1**).

4. Analysis of methylation sequencing data

Methylation sequence reads were obtained from Illumina HiSeq 2500 with paired-end reads of 125 bp in read length. Prior to the analysis, the raw sequences were processed and trimmed as previously described [22,23]. The trimmed short reads were mapped to the human reference genome (hg19) downloaded from the UCSC Genome Browser (http://hgdownload.soe.ucsc.edu/goldenPath/hg19/database/) using bowtie2 (2.2.4) [24] and Bismark (v0.16.1) [25]. For each CpG site, the 5mC rate was calculated as the percentage of unconverted cytosines in each library. Bisulfite conversion rates were estimated from the number of unconverted cytosines at Klenow filled-in 3'MspI sites of sequencing reads that were short enough to read through these sites.

Next, we used metilene software (Version 0.23) [26] to identify differentially methylated regions (DMRs) between A2780-C9 and A2780-E8. The final DMRs were determined using the following threshold: at least ten CpG sites in the DMRs, at least 10% differences in methylation levels between the two tested groups, and false discovery rate (FDR)<0.05. These DMR regions were divided into three categories: transcription start site (TSS), intergenic and intragenic regions. TSS regions were defined as 1 kb upstream and downstream of TSS of a transcript (UCSC gene annotation, hg19). Genes with promoter regions overlapping with TSS DMR were subjected to gene ontology (GO) and pathway analysis using clusterporfilter [27].

5. Library preparation for RNA sequencing

Transcriptome analysis of ovarian cancer cells A2780-C9 and A2780-E8 was conducted using RNA-seq as described previously [28]. Three biological replicates were done for each cell subline. Briefly, total RNA was isolated using TRIzol according to the manufacturer's instructions (Invitrogen, Carlsbad, CA, USA). cDNA libraries were prepared using a TruSeq RNA Sample Preparation Kit (Illumina). Libraries were quantified using quantitative polymerase chain reaction (qPCR) according to the Illumina's qPCR quantification guide to ensure uniform cluster density. Samples were multiplexed and paired-end sequenced with an Illumina HiSeq X10 (**Table S2**).

6. Analysis of RNA-seq data

Transcriptome data were mapped to human reference genome (hg19) and gene annotation database (Ensembl genes v75) using Tophat v2 (v2.0.13) with the spliced mapping algorithm [29]. A set of both known and novel transcripts was constructed and identified using Cufflinks [30]. Gene expression was quantified using fragments per kilobase of transcript per million reads mapped. Finally, differentially expressed genes (DEGs) between ovarian cancer cells with low and high metastatic potentials (FDR<0.05) were determined by Cuffdiff [30].

7. Targeted bisulfite sequencing assay

MethylTarget™ assays (targeted bisulfite sequencing) were carried out to verify the methylation changes at DMRs according to the protocols developed by Genesky BioTech (Shanghai, China). Briefly, DNA samples were first treated with sodium bisulfite and subsequently enriched. Then, multiplex PCR primers were designed for simultaneous amplification of multiple DMRs (Genesky BioTech, China) (**Tables S3** and **S4**). Finally, amplified DNA samples were indexed for multiplexing and used for preparing for sequencing library according to the Illumina protocols. Methylation sequencing libraries were sequenced on an Illumina HiSeq 2500 sequencer.

8. Human ovarian cancer samples

To evaluate the DNA methylation changes identified in ovarian cancer cell lines, 19 pairs of peritoneal metastatic ovarian carcinoma tissues and matched primary ovarian carcinoma tissues were obtained from the surgical specimen archives of the Women's Hospital of Zhejiang University School of Medicine (**Table S5**). Tissue specimens were snap-frozen in liquid nitrogen and stored at −80°C for RNA extraction. Hematoxylin and eosin slides were reviewed by a pathologist to confirm the diagnosis.

9. Real-time quantitative reverse transcription polymerase chain reaction (RT-qPCR)

One microgram total RNA extracted from cell lines or human tissues using Trizol was reverse transcribed into cDNA in a reaction volume of 20 μL using PrimeScript™ RT reagent Kit with gDNA Eraser (TAKARA, Shiga, Japan). Primers for real-time qRT-PCR analysis of SFRP1 and LIPG, and GAPDH are provided in **Table S6**. Before the analysis, total RNA was incubated at 37°C for 10 minutes with or without RNase R exonuclease (NEB).

10. 5-aza-dC treatment

A2780-C9 cells were seeded in a 6-well plate (2×10^5/well) for one day and then treated with 5-aza-2'-deoxycytidine (Sigma) at different final concentrations for 4 days. Culture medium was changed every 2 days with new drugs added. Cell pellets were harvested for RNA extraction. mRNA expression levels of target genes were evaluated in comparison to the endogenous control gene GAPDH using RT-qPCR.

11. Western blot

Cells were suspended in lysis buffer (50 mM Tris-HCl PH 8.0, 1% SDS, 1 mM EDTA, 5 mM DTT, 10 mM PMSF, 1 mM NaF, 1 mM Na_3VO_4, and protease inhibitor cocktail), and then denatured in boiling water for 10 minutes. The cellular lysates were centrifuged at 13,000 rpm for 30 minutes. The protein concentration was determined using a BCA assay (Thermo Fisher Scientific). Equal amount of proteins (40 μg) was used to perform sodium dodecyl polyacrylamide gel electrophoresis (SDS-PAGE) using 10% gel. The proteins were then transferred onto a polyvinylidene fluoride membrane. The membrane was blocked with 5% skim milk and incubated with the antibodies. The antibodies used included rabbit anti-SFRP1 and anti-LIPG2 (**Table S6**). Immunoreactive bands were developed by enhanced chemiluminescence reaction (Pierce, Thermo Fisher Scientific) following standard protocols.

12. Knockdown of SFRP1 and LIPG

Small interference RNAs (siRNAs) targeting SFRP1 and LIPG were designed and synthesized by GenePharma (Shanghai, China) (**Table S6**). A2780-E8 and OVCAR3 cells were cultured in RPMI medium 1640 supplemented with 10% FBS. Cells were transfected with these siRNAs with GeneMute™ reagent (SignaGen Laboratories, Rockville, MD, USA). All transfection assays were carried out in triplicate.

13. Overexpression of SFRP1 and LIPG

SFRP1 and LIPG were amplified by PCR from Hela cell cDNA and subcloned into the BamHI/XhoI site of the pENTER expression vector. Then constructed vectors were transfected into ovarian cancer cells. In brief, A2780-C9 cells were maintained in RPMI1640 medium supplemented with 10% FBS, and TOV112D cells were maintained in DMEM medium (Gibco) supplemented with 10% FBS. Cells were plated at a density of $2.0×10^4$ cells/well in a 6-well plate for 24 hours, and then transfected with 1.5 μg of total plasmid DNA together with 3.75 μL of Lipofectamine™ 3000 reagent (Life) per well. Cells were subjected to in vitro studies 24 hours after transfection.

14. CCK8 assay

Cell proliferation was tested with the CCK8 kit (DOJINDO, Kumamoto, Japan). Cells were seeded in 96-well plates with approximate 2,000 cells/well in 100 μL medium in quintuplicate. CCK8 was added into wells at 0, 24, 48, 72, 96, and 120 hours respectively, and incubated for 2.5 hours. The absorbance was measured at a wavelength of 450 nm.

15. Animal experiments

Five-week-old female athymic nude mice (BALB/c Nude) were used for the xenograft model. A2780-C9 cells stably expressing SFRP1 (OV-SFRP1) or empty vector (EV) were dissociated using trypsin and washed twice with sterilized PBS. Then, 0.2 mL of PBS containing $3×10^6$ cells was subcutaneously inoculated into the flank of mice. Mice were monitored every 3 days for tumor growth, and the tumor size was measured using a caliper. Three weeks after inoculation, the mice were sacrificed adhering to the policy on the humane treatment of tumor-bearing animals. For tumor invasion in vivo assay, cells were first infected with HBLV-Luc-BSD virus (HANBIO, Shanghai, China) and selected with BSD (InvivoGen, San Diego, CA, USA) to obtain cells stably expressing firefly luciferase (labelled for Luc). Then, $2×10^6$ A2780-C9-luc-OV SFRP1 cells and A2780-C9-luc-EV cells were injected intravenously into the tail vein. $2×10^6$ A2780-C9-Luc cells and A2780-E8-Luc cells were injected intraperitoneally into nude mice. Five minutes following injection, 1.5 mg luciferin (Gold Biotech, St Louis, MO, USA) was administered to monitor metastases using an IVIS@ Lumina II system (Caliper

Life Sciences, Hopkinton, MA, USA). All experiments were performed in accordance with the Guide for the Care and Use of Laboratory Animals (NIH publication 80-23, revised 1996), with the approval of the Zhejiang University, Hangzhou, China.

16. Statistical analysis

The differences between two groups were examined using Student's t-test for normally distributed data and Mann–Whitney U test for non-normally distributed data. The value of p<0.05 were considered statistically significant. The events of overall survival were defined as death, while recurrence-free survival was ended by any disease recurrence, or death. Before the survival analysis, the mean of expression of SFRP1 or LIPG was used to classify patient samples into two groups. Survival distributions in two different groups were visualized using Kaplan-Meier curves. Differences in overall survival and recurrence-free survival between the two groups were assessed by a log-rank test. All statistical analyses were implemented in R statistical packages (https://www.r-project.org/).

17. Ethics approval and consent to participate

This study was reviewed and approved by the Ethnics Committees of Women's Hospital of Zhejiang University School of Medicine (Hangzhou, China). The study was conducted in accordance with the International Ethical Guidelines for Biomedical Research Involving Human Subjects. All subjects provided informed consent to participate in the study.

RESULTS

1. Establishing ovarian cancer cell lines with low- and high-metastasis potentials

Due to tumor cell heterogeneity in ovarian cancer, two monoclonal cell sublines with significant differences in metastatic potentials were isolated from a commonly used ovarian cancer cell A2780 by limiting dilution and matrigel invasion and migration assays (**Fig. 1A**). Briefly, A2780 cells at log phase were diluted to a density of 10/mL and seeded into a 96-well plate. Next, a marker was added on the well containing a single cell under a microscope. Then, these single cell wells were being cultured for 2–3 weeks, and good clones were selected and amplified for subsequent assays. Finally, the metastatic potentials of these clones were evaluated using transwell migration and invasion assays. As a result, one cell subline with the highest potential of metastasis (i.e., A2780-C9) and one cell subline with the lowest potential of metastasis (i.e., A2780-E8) were established; the metastatic ability of subline A2780-C9 was about 1.5 times higher than the parental cell A2780, and 4 times higher than subline A2780-E8 (**Fig. 1B**). The observed differences in the metastatic potentials of A2780-C9 and A2780-E8 in vitro (**Fig. S1**) and in vivo (**Fig. 1C**) were maintained after several passages. These two newly established sublines were subsequently utilized to investigate the potential epigenetic mechanisms underlying ovarian cancer metastasis in the subsequent experiments.

2. DNA methylation changes associated with ovarian cancer metastasis

To assess if changes in DNA methylation can contribute to ovarian cancer metastasis, we analyzed genome-wide DNA methylation profiles of these two cell sublines using RRBS technology [21]. Six samples were used for RRBS library preparation with three biological replicates per subline. The bisulfite conversion rate was 99.9% (**Table S1**). On average, 16 million reads were generated and 1,810,698 CpG sites with at least 5X coverage were identified in each library. CpG sites were removed if they were in the heterosomes and

overlapped with the Database of single nucleotide polymorphisms (dbSNP build 142), and the remaining 1,682,816 CpG sites that covered at all six samples were used for downstream analyses. To assess the reproducibility of RRBS, the genome-wide CpG methylation levels between each sample were compared. The average Pearson's correlation coefficient between biological replicates was 0.98 (p<0.001) (**Fig. S2A**), indicating high reproducibility of RRBS in our experiments.

Unsupervised hierarchical clustering was performed using the top 10,000 of CpG sites that varied most across all the samples. As expected, the six samples were clearly segregated into two groups, one representing the subline A2780-C9 and the other one representing the subline A7280-E8 (**Fig. 2A**). This indicates that there are distinct global DNA methylation patterns between ovarian cancer cell lines with low- and high-metastasis. Next, we identified individual DMRs between the two sublines with low- and high-metastasis. In total, 313
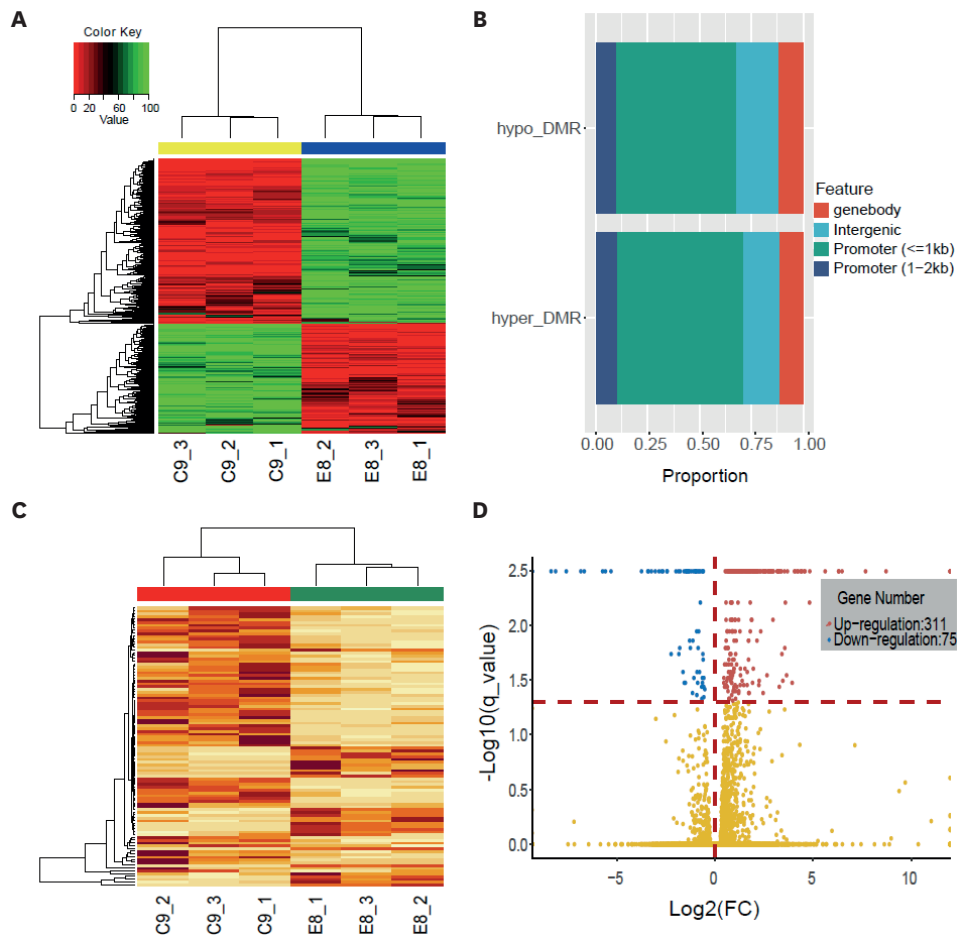
Fig. 2. Distinct DNA methylation and gene expression patterns between ovarian cancer cell lines with low- and high-metastasis. (A) Unsupervised hierarchical clustering based on methylation levels of the top 10,000 CpG sites. Each row represents a CpG site, and each column depicts methylation data from a single sample. Six samples were clustered into two experimental groups, one representing the subline A2780-C9 and the other one representing the subline A7280-E8. (B) Distribution of hyper- and hypo-DMRs. DMRs refer to genomic regions that are differentially methylated between high-metastatic C9 and low-metastatic E8. Hyper- and hypo-DMRs are DMRs that are hypermethylated and hypomethylated, respectively, in high-metastatic C9 cells compared to low-metastatic E8 cells. (C) Unsupervised hierarchical clustering of the samples based on gene expression profiles. Similarly, clustering of the samples based on the gene expression data corresponded well with the experimental grouping. (D) Scatterplot showing the relative expression of mRNA and the statistical significance of differential expression analysis between ovarian cancer sublines with low and high metastatic potentials. FC represents fold change, that is, the ratio of mRNA expression in in high-metastatic C9 to that in in low-metastatic E8. q values are adjusted p values from the differential expression analysis.
CpG, cytosine-phosphate-guanine; DMR, differentially methylated region.

hypermethylated DMRs (hyper-DMRs) and 559 hypomethylated DMRs (hypo-DMRs) were detected in high-metastatic C9 compared to low-metastatic E8 (FDR<0.05). Among them, approximately 60% of these DMRs were located in gene promoter regions, suggesting their large potential impacts on gene regulation (**Fig. 2B**). Then, we performed GO and pathway enrichment analyses for genes whose promoter regions overlapped with these DMRs. Many GO terms significantly enriched for DMR-associated genes are related with cell population proliferation and epithelial cell differentiation, and pathways such as adipogenesis (**Fig. S2B**).

3. Gene expression changes associated with ovarian cancer metastasis

We analyzed gene expression profiles in the same set of samples from these two cell sublines using RNA-seq technology to evaluate if changes in gene expression can also contribute to ovarian cancer metastasis. On average, approximately 57 million reads were generated, and 89% of these reads were uniquely mapped to human reference genome (hg19) in each library (**Table S2**). Across these cell sublines, 11,788 transcripts with at least one FPMK were identified. The average Pearson's correlation coefficient between biological replicates was 0.98 (p<0.001) (**Fig. S2C**), indicating high reproducibility of RNA-seq in our experiments.

Clustering of the samples based on gene expression profiles was consistent with the experimental grouping of the samples (**Fig. 2C**), suggesting distinct gene expression patterns between high- and low- metastatic sublines. In total, 311 genes were significantly upregulated, and 75 genes downregulated in in high-metastatic A2780-C9 compared to low-metastatic A2780-E8 (FDR<0.05) (**Fig. 2B**). These DEGs were significantly enriched in GO terms such as cell population proliferation, cell-cell adhesion and positive regulation of cell motility, and pathways such as extracellular matrix organization, P53 and MAPK signaling (**Fig. S2D**). Taken together, many systemic and important epigenetic and transcriptomic alterations have been detected between the A2780 sublines, as reflected by GO and pathway analyses, which may be involved in ovarian cancer metastasis.

4. Integrated analysis of DNA methylome and transcriptome

Next, we performed integrated analysis of DNA methylome and transcriptome profiles to identify methylation-induced driver genes potentially involved in ovarian cancer metastasis. According to the relationship between DEGs (FDR<0.05) and DMRs (FDR<0.05), four groups of genes were identified (**Fig. 3A**): (a) genes that are significantly hypo-methylated and down-regulated in high-metastatic cells (i.e., A2780-C9) compared to low-metastatic cells (i.e., A2780-E8); (b) genes that are significantly hypo-methylated and up-regulated in high-metastatic cells compared to low-metastatic cells; (c) genes that are significantly hyper-methylated and up-regulated in high-metastatic cells compared to low-metastatic cells; and (d) genes that are significantly hyper-methylated and down-regulated in high-metastatic cells compared to low-metastatic cells. The number of genes in these four groups were 4, 26, 8 and 7, respectively. Methylation of gene promoter often leads to repression of promoter-associated gene expression, which manifests as a negative correlation between gene expression and its promoter methylation level [3,4]. Therefore, 33 genes from groups (b) and (d) that showed an inverse relationship between their gene expression and promoter methylation are methylation-driven genes potentially associated with ovarian cancer metastasis.

Then, we performed pathway enrichment analysis of 33 methylation-driven genes (i.e., genes with negative correlation between their mRNA expression and promoter methylation) (**Table S3**). It was observed that these methylation-induced genes are enriched in multiple cancer-related pathways such as MAPK and positive regulation of cell cycle (**Fig. S3**). Notably,

twelve genes were specifically involved in five cancer-related metastasis pathways, including TMSB4X, ADAM23, LIPG, DUSP4, FLNC, HSPB1, COMP, SFRP1, FOSL1, CLEC11A, PDGFB and CFS1 (**Fig. 3B**).
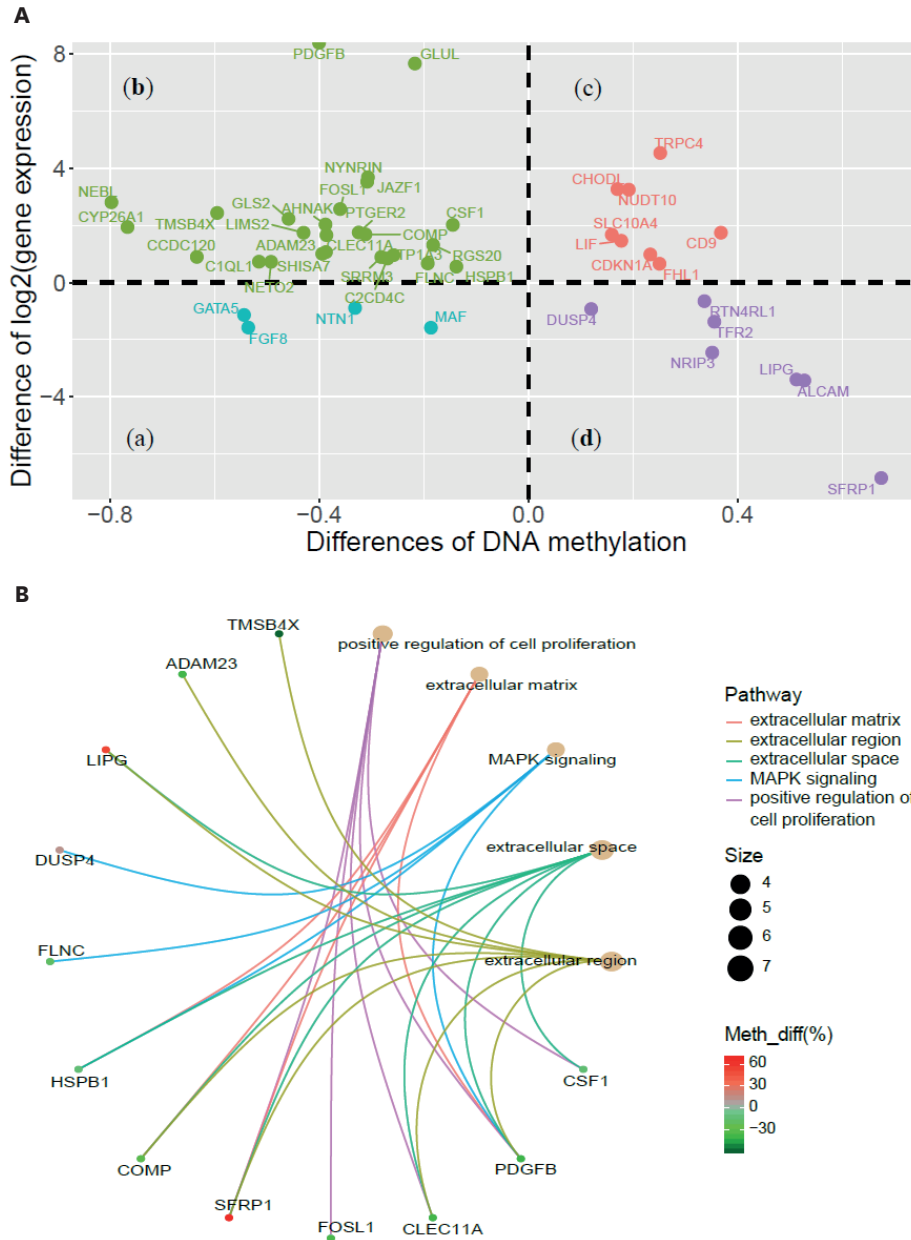
Fig. 3. Integrated analysis of DNA methylome and transcriptome identified methylation-driven genes potentially associated with ovarian cancer metastasis. (A) Starburst plot showing differential DNA methylation versus differential gene expression. Group (a): Light blue indicates that gene is significantly hypo-methylated and down-regulated in high-metastatic cells (i.e., A2780-C9) compared to low-metastatic cells (i.e., A2780-E8). Group (b): Light green circle indicates that gene is significantly hypo-methylated and upregulated in high-metastatic cells compared to low-metastatic cells. Group (c): Orange circle indicates that the gene is significantly hyper-methylated and upregulated in high-metastatic cells compared to low-metastatic cells. Group (d): Purple circle indicates that gene is significantly hyper-methylated and downregulated in high-metastatic cells compared to low-metastatic cells. According to the well-known inverse correlation between gene expression and its promoter methylation level, genes in groups (b) and (d) are methylation-driven genes that are potentially associated with ovarian cancer metastasis. (B) Circular visualization of 12 methylation-driven genes enriched in five pathways likely involved in cancer metastasis.

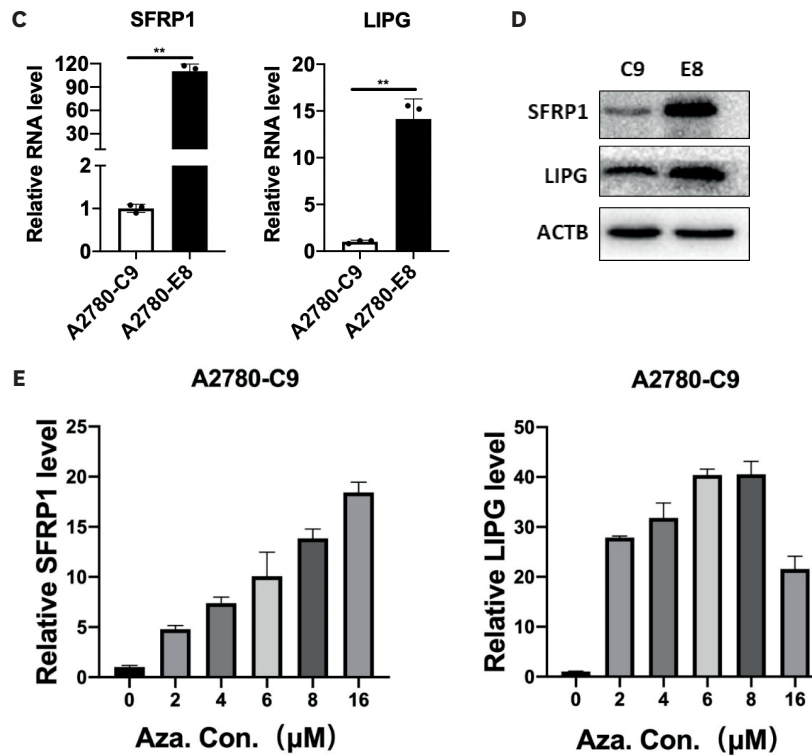## 5. SFRP1 and LIPG are two major candidates for ovarian cancer metastasis

To verify the DNA methylation changes detected in these 12 methylation-driven genes, we performed targeted bisulfate sequencing in the low- and high- metastatic sublines (**Table S4**). However, the PCR probes of two genes were not designed successfully for DMR regions in targeted bisulfate sequencing. Nine of ten remaining genes were verified to show similar trends in methylation changes between these two cell sublines (**Figs. 4A** and **S4A**). We further evaluated these nine genes in an independent cohort with primary ovarian carcinomas (i.e., tumor tissues with low-metastasis potentials) and matched peritoneal metastatic ovarian carcinomas (i.e., tumor tissues with high-metastasis potentials) (**Figs. 4B** and **S4B**). Among them, the DNA methylation changes of Secreted Frizzled Related Protein 1 (SFRP1) and Lipase G (LIPG) between the two cell sublines were consistent with their changes between primary ovarian carcinomas and matched peritoneal metastatic ovarian carcinomas. However, CSF1 showed reverse trend in changes of DNA methylation in ovarian tumor tissues. The other ones did not show significant methylation difference between primary ovarian carcinomas and matched peritoneal metastatic ovarian carcinomas.
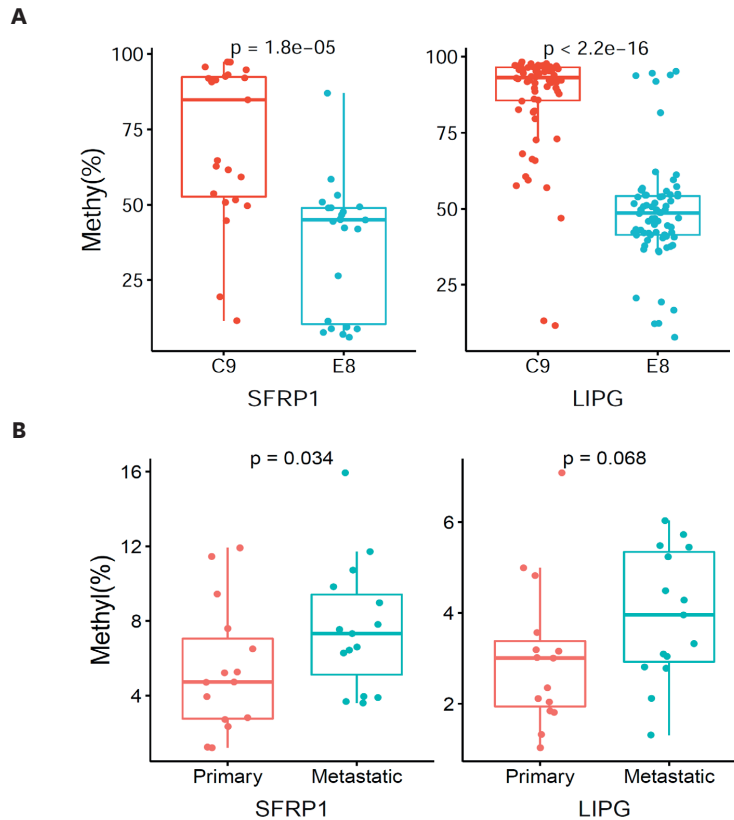
Fig. 4. SFRP1 and LIPG are major candidates for methylation-induced genes in ovarian cancer metastasis. (A) Methylation levels of SFRP1 and LIPG in low- (i.e., A2780-E8) and high-metastatic sublines (i.e., A2780-C9), validated by targeted bisulfite sequencing. Each point represents one cytosine-phosphate-guanine site within differentially methylated regions that showed differential methylation levels between A2780-C9 and A2780-E8. The thick line in the boxplot is median and the box spans from Q1 (25th percentile) to Q3 (75th percentile). (B) Methylation levels of SFRP1 and LIPG in an independent cohort of ovarian cancer, validated by targeted bisulfite sequencing. Methylation levels of SFRP1 and LIPG promoters were measured in 19 primary ovarian carcinoma (i.e., low metastatic potential) and matched peritoneal metastatic ovarian carcinomas (i.e., high metastatic potential). Each point represents one sample.
**p<0.01.

Fig. 4. (Continued) SFRP1 and LIPG are major candidates for methylation-induced genes in ovarian cancer metastasis. (C) SFRP1 and LIPG mRNA expression levels in A2780-C9 and A2780-E8 cells, determined by qRT-PCR. (D) SFRP1 and LIPG protein levels in A2780-C9 and A2780-E8 cells, determined by western blot. (E) SFRP1 and LIPG expression was increased in A2780-C9 cells after 5-aza-dC treatment. The relative expression of SFRP1 and LIPG in A2780-C9 cells treated with increasing concentrations of 5-aza-dC was determined by qRT-PCR. Data are presented as mean ± SD; n=3.
qRT-PCR, quantitative reverse transcription polymerase chain reaction.
**p<0.01.

SFRP1 and LIPG were hypermethylated in their gene promoters and downregulated in their mRNA levels and protein levels in the high-metastatic subline (i.e., A2780-C9) compared with the low-metastatic subline (i.e., A2780-E8) (**Figs. 4C** and **4D**). Therefore, we further examined the consequence of demethylation on the expression of SFRP1 and LIPG using the demethylating agent 5-aza-dC in the high-metastatic subline (i.e., A2780-C9). The expression of SFRP1 and LIPG was found to be strongly upregulated in A2780-C9 cells after treatment of 5-aza-dC (**Fig. 4E**), suggesting that the expression of SFRP1 and LIPG is potentially regulated by their promoter methylation.

In human ovarian cancer, compared to primary ovarian tumor tissues, the DNA methylation levels of SFRP1 and LIPG in matched peritoneal metastatic ovarian tumor tissues were higher (**Fig. 4B**), but their gene expression levels were lower (**Fig. S5A and B**). This change trend was very similar to that observed in A2780 sublines, suggesting a functional relevance of SFRP1 and LIPG to human ovarian cancer. Furthermore, we assessed expression of SFRP1 and LIPG in tissues from ovarian cancer patients with clinical outcome using microarray data downloaded from Gene Expression Omnibus (GSE9891 and GSE73614). Kaplan–Meier survival analysis revealed that patients with lower SFRP1 (**Fig. S5C, E and G**) or LIPG (**Fig. S5D, F and H**) expression tend to have a worse prognosis. These data suggested that SFRP1 and LIPG are valuable prognostic biomarkers, although validation in an independent large sample is warranted, and may play a tumor suppressive role in ovarian cancer progression.

6. Validation of the function of SFRP1 and LIPG in ovarian cancer metastasis

Finally, we performed loss-of-function and gain-of-function in vitro assays to investigate the tumor suppressive roles of SFRP1 and LIPG in ovarian cancer cells. SFRP1 and LIPG were highly abundant in low-metastatic subline E8, whereas they were largely downregulated in high-metastatic subline C9 (**Fig. 4C and D**). Thus, we knocked down SFRP1 and LIPG by transfecting siRNA into the A2780-E8 subline (**Fig. 5A and B**). Knockdown of SFRP1 and LIPG expression significantly promoted cell growth in E8 cells compared to the non-targeting control siRNAs (**Fig. 5C**). Transwell assays also revealed that inhibition of SFRP1 and LIPG expression significantly increased cell migration in A2780-E8 cells compared with the non-targeting control siRNAs (**Fig. 5D**). Next, we over-expressed SFRP1 and LIPG by subcloning these genes into a pENTER expression vector in the A2780-C9 subline (**Fig. 5E and F**). Overexpression of SFRP1 and LIPG significantly inhibited cell growth and migration in A2780-C9 compared with the EV (**Fig. 5G and H**). Collectively, these findings suggest that SFRP1 and LIPG play a role in tumor suppression in ovarian cancer cells, which is dependent on promoter hypermethylation.

SFRP1 is a secreted antagonist of Wnt signaling. We thus evaluated if epigenetic silencing of SFRP1 can affect Wnt signaling in ovarian cancer. As expected, knockdown of SFRP1 caused an increase in phosphorylated GSK3β and an increase in β-catenin expression, leading to deregulated activation of the Wnt pathway; whereas overexpression of SFRP1 resulted in the opposite effects on the Wnt signaling (**Fig. 5I and J**). To further examine the function of SFRP1 in vivo, we subcutaneously injected A2780-C9 cells with stable overexpression of SFRP1 (OV-SFRP1) and empty vector control (EV) into the nude mice. The volume and weight of tumor in the SFRP1 overexpression group were significantly smaller than the control group (**Figs. 5K**, **S6A and B**). To explore the tumor-suppressive effect of SFRP1 on ovarian cancer cell metastasis in vivo, we first obtained a cell line stably expressing luciferase (A2780-C9-luc), and used A2780-C9-luc to select cells stably overexpressing SFRP1. Finally, we intravenously injected A2780-C9-luc-OV SFRP1 and A2780-C9-luc-EV cells into the lateral tail veins of nude mice. We observed that overexpression of SFRP1 significantly reduced ovarian cancer cell metastasis in vivo (**Figs. 5L** and **S6C**). These data suggest that SFRP1 can inhibit tumorigenicity and metastasis of ovarian cancer cells in vivo.

Since these two sublines were derived from the parental cell line A2780, we further assessed whether SFRP1 and LIPG have similar tumor suppressive functions in other ovarian cancer cell lines such as TOV12D and OVCAR3 (**Fig. 6A and B**). Both SFRP1 and LIPG were highly expressed in OVCAR3 cells. Therefore, we knocked down SFRP1 and LIPG using siRNAs in OVCAR3 cells (**Fig. 6C and D**). Consistently, knockdown of SFRP1 or LIPG promoted proliferation and migration of ovarian cancer cells (**Fig. 6E and F**). In contrast, we overexpressed SFRP1 and LIPG in TOV112D, where the endogenous expression levels of SFRP1 and LIPG were low (**Fig. 6G and H**). As expected, ectopic expression of SFRP1 or LIPG suppressed ovarian cancer cell proliferation and migration (**Fig. 6I and J**). These results further confirmed the general tumor suppressive function of SFRP1 and LIPG in ovarian cancer cells.

DISCUSSION

A recent single-cell RNA sequencing study has revealed substantial heterogeneity within diverse cancer cell lines and identified recurrent patterns of heterogeneity that are shared
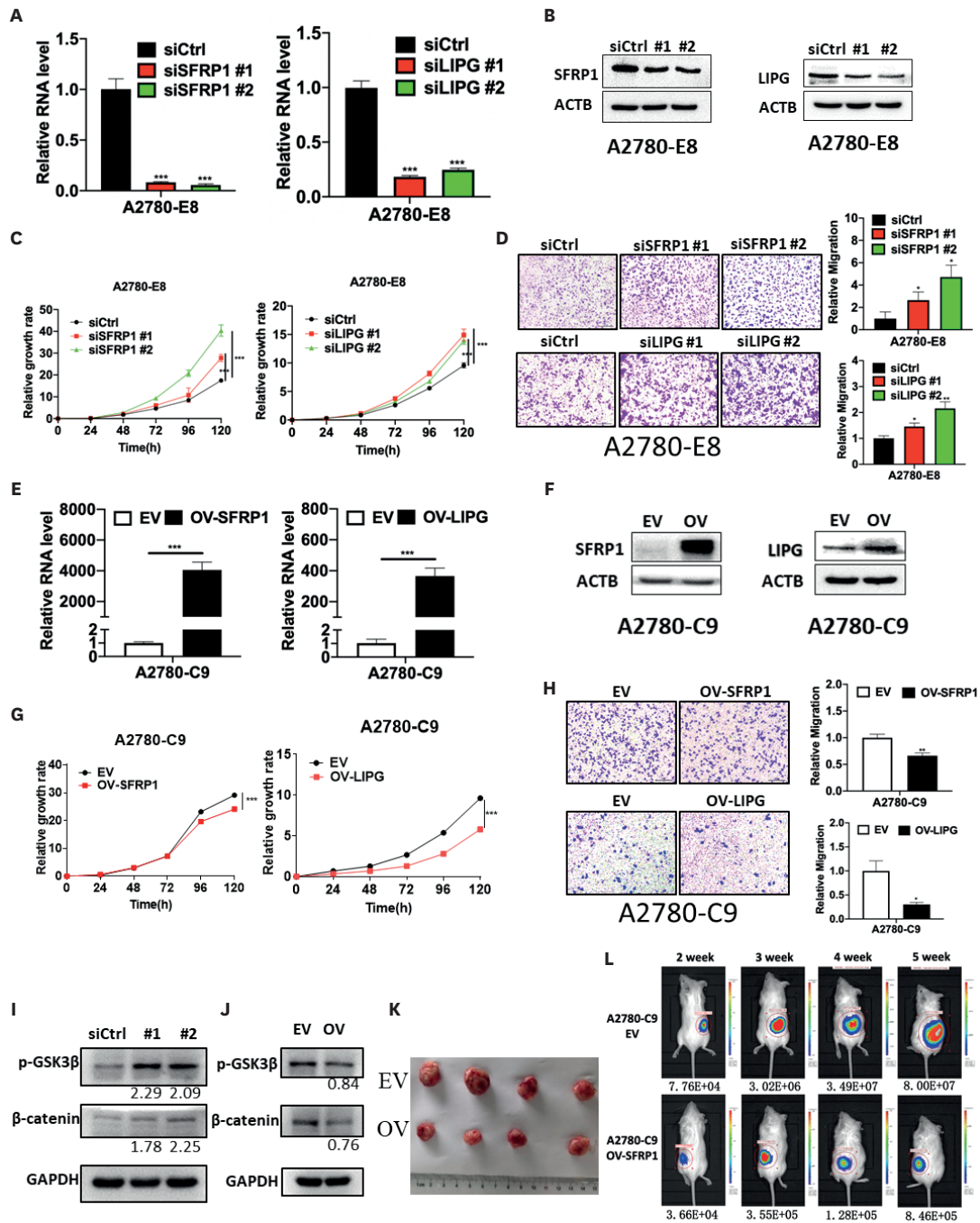
Fig. 5. SFRP1 and LIPG act as tumor suppressors in A2780 sublines. (A) qRT-PCR analyses of SFRP1 and LIPG expression levels in A2780-E8 cells transfected with SFRP1 siRNAs, LIPG siRNAs, or control. (B) Western blot analyses of SFRP1 and LIPG protein levels in A2780-E8 cells transfected with SFRP1 siRNAs, LIPG siRNAs, or control. (C) CCK8 assays for A2780-E8 cells transfected with SFRP1 siRNAs, LIPG siRNAs, or control. (D) Transwell migration assays for A2780-E8 cells transfected with SFRP1 siRNAs, LIPG siRNAs, or control. (E) qRT-PCR analyses of SFRP1 and LIPG expression levels in A2780-C9 cells transfected with SFRP1 OV, LIPG OV, or EV. (F) Western blot analyses of SFRP1 and LIPG protein levels in A2780-C9 cells transfected with SFRP1 OV, LIPG OV, or EV. (G) CCK8 assays for A2780-C9 cells transfected with SFRP1 OV, LIPG OV, or EV. (H) Transwell migration assays for A2780-C9 cells transfected with SFRP1 OV, LIPG OV, or EV. (I) Western blot analyses of p-GSK3β and β-catenin protein levels in A2780-E8 cells transfected with SFRP1 siRNAs or control. (J) Western blot analyses of p-GSK3β and β-catenin protein levels in A2780-C9 cells transfected with SFRP1 OV or EV. (K) SFRP1 inhibits ovarian tumor growth in vivo (n=4). A2780-C9 cells stably expressing SFRP1 OV or EV were subcutaneously inoculated into the flank of nude mice. The tumor growth curve was measured every 3 days. (L) SFRP1 inhibits ovarian cancer metastasis in vivo (n=4). Representative images from the metastatic assay are shown from the second to the fifth week. A2780-C9-luc cells stably expressing SFRP1 OV or EV were injected intravenously into the tail vein of nude mice. Luciferin was administered to monitor metastasis using an IVIS@ Lumina II system. Data are presented as mean ± SD; n=3.
EV, empty vector; OV, overexpression vector; qRT-PCR, quantitative reverse transcription polymerase chain reaction.
**p<0.01, ***p<0.001.
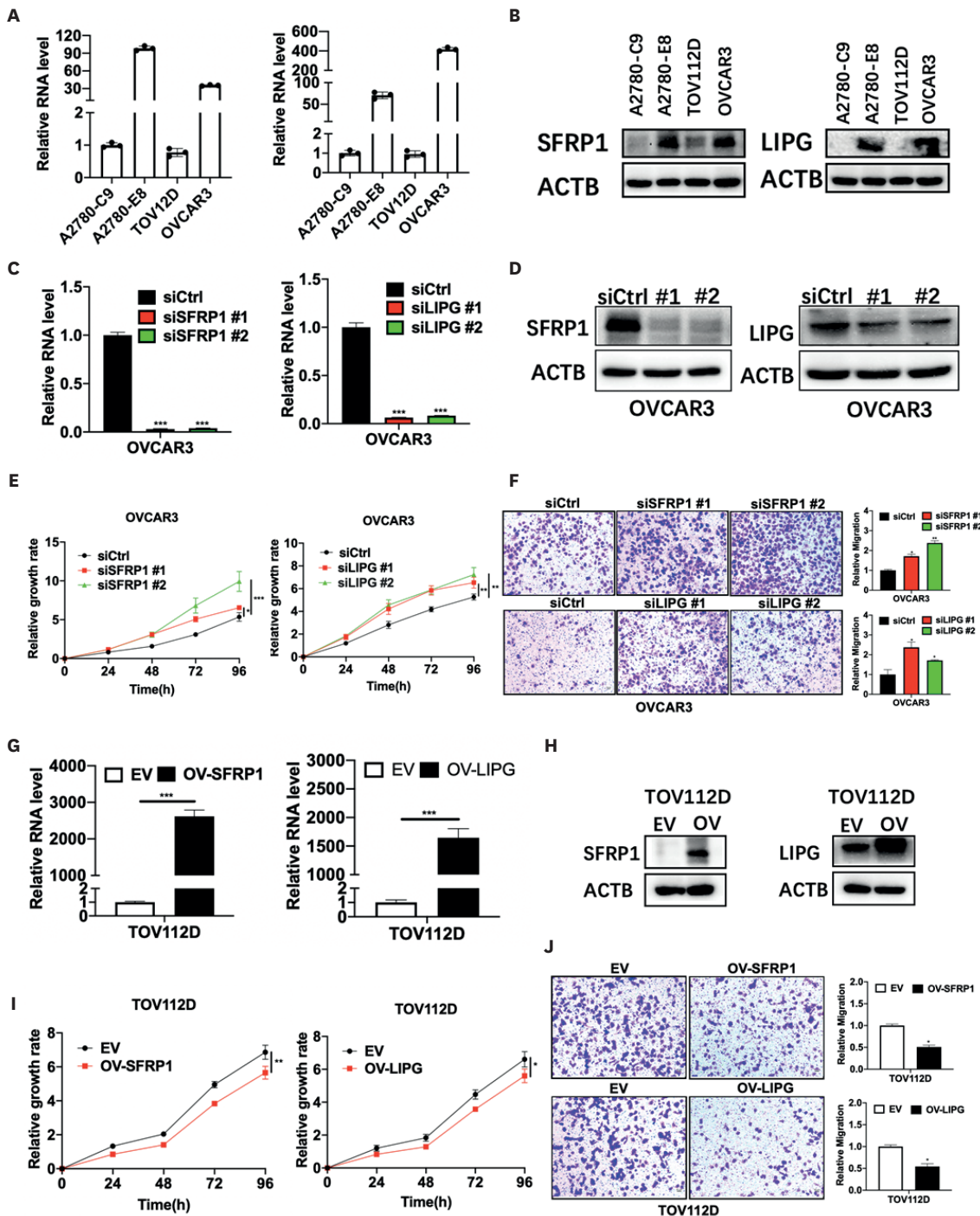
Fig. 6. Further validation of tumor suppressor functions of SFRP1 and LIPG in other ovarian cancer cell lines. (A) SFRP1 and LIPG mRNA expression levels in ovarian cancer cells (A2780-C9, A2780-E8, OVCAR3 and TOV112D), determined by qRT-PCR. (B) SFRP1 and LIPG protein levels in ovarian cancer cells, determined by western blot. (C) qRT-PCR analyses of SFRP1 and LIPG expression levels in OVCAR3 cells transfected with SFRP1 siRNAs, LIPG siRNAs, or control. (D) Western blot analyses of SFRP1 and LIPG protein levels in OVCAR3 transfected with SFRP1 siRNAs, LIPG siRNAs, or control. (E) CCK8 assays for OVCAR3 cells transfected with SFRP1 siRNAs, LIPG siRNAs, or control. (F) Transwell migration assays for OVCAR3 cells transfected with SFRP1 siRNAs, LIPG siRNAs, or control. (G) qRT-PCR analyses of SFRP1 and LIPG expression levels in TOV112D cells transfected with SFRP1 OV, LIPG OV, or EV. (H) Western blot analyses of SFRP1 and LIPG protein levels in TOV112D cells transfected with SFRP1 OV, LIPG OV, or EV. (I) CCK8 assays for TOV112D cells transfected with SFRP1 OV, LIPG OV, or EV. (J) Transwell migration assays for TOV112D cells transfected with SFRP1 OV, LIPG OV, or EV. Data are presented as mean ± SD; n=3.
EV, empty vector; OV, overexpression vector; qRT-PCR, quantitative reverse transcription polymerase chain reaction.
**p<0.01, ***p<0.001.

between tumors and specific cell lines [31]. In the present study, we first performed single cell cloning of the A2780 ovarian cancer cell line and established two cell sublines (A2780-E8 and A2780-C9) with significantly different metastatic abilities. Next, we carried out DNA methylome and transcriptome profiling in these two cell sublines. There are distinct DNA methylation and gene expression patterns between the two cell sublines with low- and high-metastasis potentials. Integrated analysis of DNA methylome and transcriptome identified 33 genes with aberrant DNA methylation that are potentially associated with ovarian cancer metastasis. Then, DNA methylation patterns of these genes were further validated in ovarian cancer tissues. Among them, SFRP1 and LIPG were hyper-methylated in A2780-C9 (high-metastatic potential) compared to A2780-E8 (low-metastatic potential). They were also hyper-methylated in peritoneal metastatic ovarian carcinomas compared to primary ovarian carcinomas. Ovarian cancer patients with lower SFRP1 and LIPG tended to have a worse prognosis. Finally, cell-based in vitro and in vivo assays were subsequently conducted to confirm the tumor suppression role of SFRP1 and LIPG in ovarian cancer cells. Functionally, knockdown of SFRP1 and LIPG promoted cell growth and migration, whereas their overexpression resulted in the opposite effects. In particular, knockdown of SFRP1 led to an increase in phosphorylated GSK3β and an increase in β-catenin expression, leading to deregulated activation of the Wnt-pathway.

SFRP1 encodes for a member of the Secreted Frizzled Related Protein (SFRP) family that contains a cysteine-rich domain homologous to the putative Wnt-binding site of Frizzled proteins. Members of this family act as soluble modulators of Wnt signaling and play important roles in various biological processes such as cell proliferation, migration, invasion, and differentiation. Among the SFRP members, epigenetic silencing of SFRP1 has been described in multiple malignancies, including hepatocellular carcinoma [32], breast cancer [33], and non-small cell lung cancer [34]. Our study revealed that the promoter hyper-methylation of SFRP1 may contribute to ovarian cancer metastasis. Mechanistically, depletion of SFRP1 resulted in deregulated activation of the Wnt-pathway, thereby contributing to the progression of ovarian cancer.

Endothelial lipase (LIPG) is a form of lipase secreted by vascular endothelial cells in tissues with high metabolic rates and vascularization, such as the liver, lung, kidney, and thyroid gland [35]. The LIPG enzyme is a vital component to many biological processes such as lipoprotein metabolism and vascular biology. However, its role in carcinogenesis and tumor progression is rarely reported. In aggressive human basal-like triple-negative breast cancer, LIPG is aberrantly overexpressed and acts as an oncogene to promote tumor initiation and metastasis [36]. On the contrary, our study showed that LIPG is hyper-methylated in peritoneal metastatic ovarian carcinomas. Depletion of LIPG promoted cell growth and migration, whereas overexpression of LIPG exerted an opposite role, suggesting that LIPG may play a tumor suppression role in ovarian cancer. The conflicting role of LIPG in tumors may be due to its context-dependent regulatory function in cancer, which is required to be further investigated in future studies.

In summary, many systemic and important epigenetic and transcriptomic alterations have been detected in the progression of ovarian cancer. In particular, SFRP1 and LIPG function as tumor suppressors in ovarian cancer and their epigenetic silencing is a potential driver event in ovarian cancer metastasis. Our data also provided new insights into epigenetic and transcriptomic alterations associated with ovarian cancer metastasis and may advance the identification of biomarkers and drug targets for predicting and controlling cancer metastasis.

ACKNOWLEDGEMENTS

SUPPLEMENTARY MATERIALS

Table S1

Quality control metrics of Reduced Representation Bisulfite Sequencing libraries

Click here to view

Table S2

Quality control metrics of RNA sequencing libraries

Click here to view

Table S3

Genes showing inverse relationship between their promoter methylation and mRNA expression

Click here to view

Table S4

Multiplex polymerase chain reaction primers used for amplifying DMRs in MethylTarget™ assays

Click here to view

Table S5

Characteristics of ovarian cancer patient samples used in the study

Click here to view

Table S6

Information on antibodies and primers used in in vitro cell assays

Click here to view

Fig. S1

Differences in the metastatic potential between A2780 sublines retained after passage. (A) A2780-C9 and A2780-E8 cells were transfected with HBLV-LUC-BSD virus to obtain cells stably expressing Firefly luciferase (termed A2780-C9-luc and A2780-E8-luc). The regions of interest for A2780-C9-luc and A2780-E9-luc cells are 1.96×10^8 and 2.22×10^8, respectively. (B) Transwell assays were performed to measure in vitro migration abilities of A2780-C9-luc and A2780-E8-luc cells.

Click here to view

Fig. S2

Reproducibility of RRBS and RNA-seq data, and GO and pathway enrichment analysis of DMR-associated genes and differentially expression genes. (A) Correlation of RRBS data between biological replicates. Numbers in boxes are Pearson's correlation coefficients. (B) GO and pathway enrichment analyses of genes containing DMRs identified as differentially methylated between A2780-C9 and A2780-E8 sublines. (C) Correlation of RNA-seq data between biological replicates. Numbers in boxes are Pearson's correlation coefficients. (D) GO and pathway enrichment analyses of genes identified as differentially expressed between A2780-C9 and A2780-E8 sublines.

Click here to view

Fig. S3

Pathway enrichment analysis of genes with inverse correlation between its mRNA expression and promoter methylation.

Click here to view

Fig. S4

Validation of methylation changes of methylation-induced genes in A2780 subline and ovarian cancer cohort by targeted bisulfite sequencing. (A) Methylation levels in gene promoters were measured in low- (i.e., A2780-E8) and high-metastatic cells (i.e., A2780-C9). The thick line in the box is median and the box spans from Q1 (25th percentile) to Q3 (75th percentile). Each point represents one cytosine-phosphate-guanine site within DMR. (B) Methylation levels in gene promoters were measured in 19 primary ovarian carcinoma and matched peritoneal metastatic ovarian carcinomas. Each point represents one sample. Only genes specifically involved in five cancer-related metastasis pathways were subjected to targeted bisulfite sequencing.

Click here to view

Fig. S5

SFRP1 and LIPG expression levels are associated with outcome of ovarian cancer patients. (A, B) SFRP1 and LIPG expression in an independent cohort of 36 pairs of primary ovarian carcinoma and matched peritoneal metastatic ovarian carcinomas. SFRP1 and LIPG expression was measured by qRT-PCR and normalized to the expression of actin. FC represents the fold change of expression of metastatic ovarian carcinomas with respect to expression of its matched primary ovarian carcinoma, i.e., FC= (expression of metastatic ovarian carcinomas) / (expression of its matched primary ovarian carcinoma). (C, E, G) Kaplan-Meier curves of OS and PFS using SFRP1 expression levels. (D, F, H) Kaplan-Meier curves of OS and PFS using LIPG expression levels. Dataset GSE9891 included 185 ovarian cancer patients with OS and PFS clinical data; Dataset GSE73614 include 106 ovarian cancer patients with PFS clinical data. Before the survival analysis, patient samples were classified into two groups according to the mean of expression of SFRP1 or LIPG in datasets. A log-rank test was used to evaluate statistical differences in survivals between the two groups.

Click here to view

Fig. S6

Effect of SFRP1 on tumor formation and metastasis in nude mice. (A) Tumor volume and (B) tumor weight of mouse xenografts. A2780-C9 cells stably expressing SFRP1 OV or EV were subcutaneously inoculated into the flank of nude mice (n=4). The tumor growth curve was measured every 3 days. (C) Quantification of photon flux for metastases of A2780-C9-luc cells stably expressing SFRP1 OV or EV in nude mice.

Click here to view

REFERENCES

1. Jayson GC, Kohn EC, Kitchener HC, Ledermann JA. Ovarian cancer. Lancet 2014;384:1376-88.
   PUBMED | CROSSREF

2. Doubeni CA, Doubeni AR, Myers AE. Diagnosis and management of ovarian cancer. Am Fam Physician 2016;93:937-44.
   PUBMED

3. Berger SL, Kouzarides T, Shiekhattar R, Shilatifard A. An operational definition of epigenetics. Genes Dev 2009;23:781-3.
   PUBMED | CROSSREF

4. Dupont C, Armant DR, Brenner CA. Epigenetics: definition, mechanisms and clinical perspective. Semin Reprod Med 2009;27:351-7.
   PUBMED | CROSSREF

5. Kulis M, Esteller M. DNA methylation and cancer. Adv Genet 2010;70:27-56.
   PUBMED | CROSSREF

6. Baylin SB, Esteller M, Rountree MR, Bachman KE, Schuebel K, Herman JG. Aberrant patterns of DNA methylation, chromatin formation and gene expression in cancer. Hum Mol Genet 2001;10:687-92.
   PUBMED | CROSSREF

7. Hentze JL, Høgdall CK, Høgdall EV. Methylation and ovarian cancer: can DNA methylation be of diagnostic use? Mol Clin Oncol 2019;10:323-30.
   PUBMED | CROSSREF

8. Singh A, Gupta S, Sachan M. Epigenetic biomarkers in the management of ovarian cancer: current prospectives. Front Cell Dev Biol 2019;7:182.
   PUBMED | CROSSREF

9. Baldwin RL, Nemeth E, Tran H, Shvartsman H, Cass I, Narod S, et al. BRCA1 promoter region hypermethylation in ovarian carcinoma: a population-based study. Cancer Res 2000;60:5329-33.
   PUBMED

10. Strathdee G, Appleton K, Illand M, Millan DW, Sargent J, Paul J, et al. Primary ovarian carcinomas display multiple methylator phenotypes involving known tumor suppressor genes. Am J Pathol 2001;158:1121-7.
    PUBMED | CROSSREF

11. Wang C, Horiuchi A, Imai T, Ohira S, Itoh K, Nikaido T, et al. Expression of BRCA1 protein in benign, borderline, and malignant epithelial ovarian neoplasms and its relationship to methylation and allelic loss of the BRCA1 gene. J Pathol 2004;202:215-23.
    PUBMED | CROSSREF

12. Wu Q, Lothe RA, Ahlquist T, Silins I, Tropé CG, Micci F, et al. DNA methylation profiling of ovarian carcinomas and their in vitro models identifies HOXA9, HOXB5, SCGB3A1, and CRABP1 as novel targets. Mol Cancer 2007;6:45.
    PUBMED | CROSSREF

13. Czekierdowski A, Czekierdowska S, Szymanski M, Wielgos M, Kaminski P, Kotarski J. Opioid-binding protein/cell adhesion molecule-like (OPCML) gene and promoter methylation status in women with ovarian cancer. Neuroendocrinol Lett 2006;27:609-13.
    PUBMED

14. Sellar GC, Watt KP, Rabiasz GJ, Stronach EA, Li L, Miller EP, et al. OPCML at 11q25 is epigenetically inactivated and has tumor-suppressor function in epithelial ovarian cancer. Nat Genet 2003;34:337-43.
    PUBMED | CROSSREF

15. Teodoridis JM, Hall J, Marsh S, Kannall HD, Smyth C, Curto J, et al. CpG island methylation of DNA damage response genes in advanced ovarian cancer. Cancer Res 2005;65:8961-7.
   PUBMED | **CROSSREF**

16. Xiao X, Cai F, Niu X, Shi H, Zhong Y. Association between P16INK4a promoter methylation and ovarian cancer: a meta-analysis of 12 published studies. PLoS One 2016;11:e0163257.
   PUBMED | **CROSSREF**

17. Wang G, Li X, Tian W, Wang Y, Wu D, Sun Z, et al. Promoter DNA methylation is associated with KLF11 expression in epithelial ovarian cancer. Genes Chromosomes Cancer 2015;54:453-62.
   PUBMED | **CROSSREF**

18. Widschwendter M, Apostolidou S, Jones AA, Fourkala EO, Arora R, Pearce CL, et al. HOXA methylation in normal endometrium from premenopausal women is associated with the presence of ovarian cancer: a proof of principle study. Int J Cancer 2009;125:2214-8.
   PUBMED | **CROSSREF**

19. Lund RJ, Huhtinen K, Salmi J, Rantala J, Nguyen EV, Moulder R, et al. DNA methylation and transcriptome changes associated with cisplatin resistance in ovarian cancer. Sci Rep 2017;7:1469.
   PUBMED | **CROSSREF**

20. Earp MA, Cunningham JM. DNA methylation changes in epithelial ovarian cancer histotypes. Genomics 2015;106:311-21.
   PUBMED | **CROSSREF**

21. Gu H, Bock C, Mikkelsen TS, Jäger N, Smith ZD, Tomazou E, et al. Genome-scale DNA methylation mapping of clinical samples at single-nucleotide resolution. Nat Methods 2010;7:133-6.
   PUBMED | **CROSSREF**

22. Liu Y, Liu P, Yang C, Cowley AW Jr, Liang M. Base-resolution maps of 5-methylcytosine and 5-hydroxymethylcytosine in Dahl S rats: effect of salt and genomic sequence. Hypertension 2014;63:827-38.
   PUBMED | **CROSSREF**

23. Sun X, Han Y, Zhou L, Chen E, Lu B, Liu Y, et al. A comprehensive evaluation of alignment software for reduced representation bisulfite sequencing data. Bioinformatics 2018;34:2715-23.
   PUBMED | **CROSSREF**

24. Langmead B, Salzberg SL. Fast gapped-read alignment with Bowtie 2. Nat Methods 2012;9:357-9.
   PUBMED | **CROSSREF**

25. Krueger F, Andrews SR. Bismark: a flexible aligner and methylation caller for Bisulfite-Seq applications. Bioinformatics 2011;27:1571-2.
   PUBMED | **CROSSREF**

26. Jühling F, Kretzmer H, Bernhart SH, Otto C, Stadler PF, Hoffmann S. metilene: Fast and sensitive calling of differentially methylated regions from bisulfite sequencing data. Genome Res 2016;26:256-62.
   PUBMED | **CROSSREF**

27. Yu G, Wang LG, Han Y, He QY. clusterProfiler: an R package for comparing biological themes among gene clusters. OMICS 2012;16:284-7.
   PUBMED | **CROSSREF**

28. Li L, Chen E, Yang C, Zhu J, Jayaraman P, De Pons J, et al. Improved rat genome gene prediction by integration of ESTs with RNA-Seq information. Bioinformatics 2015;31:25-32.
   PUBMED | **CROSSREF**

29. Kim D, Pertea G, Trapnell C, Pimentel H, Kelley R, Salzberg SL. TopHat2: accurate alignment of transcriptomes in the presence of insertions, deletions and gene fusions. Genome Biol 2013;14:R36.
   PUBMED | **CROSSREF**

30. Trapnell C, Roberts A, Goff L, Pertea G, Kim D, Kelley DR, et al. Differential gene and transcript expression analysis of RNA-seq experiments with TopHat and Cufflinks. Nat Protoc 2012;7:562-78.
   PUBMED | **CROSSREF**

31. Kinker GS, Greenwald AC, Tal R, Orlova Z, Cuoco MS, McFarland JM, et al. Pan-cancer single-cell RNA-seq identifies recurring programs of cellular heterogeneity. Nat Genet 2020;52:1208-18.
   PUBMED | **CROSSREF**

32. Huang J, Zhang YL, Teng XM, Lin Y, Zheng DL, Yang PY, et al. Down-regulation of SFRP1 as a putative tumor suppressor gene can contribute to human hepatocellular carcinoma. BMC Cancer 2007;7:126.
   PUBMED | **CROSSREF**

33. Lo PK, Mehrotra J, D'Costa A, Fackler MJ, Garrett-Mayer E, Argani P, et al. Epigenetic suppression of secreted frizzled related protein 1 (SFRP1) expression in human breast cancer. Cancer Biol Ther 2006;5:281-6.
   PUBMED | **CROSSREF**

34. Taguchi YH, Iwadate M, Umeyama H. SFRP1 is a possible candidate for epigenetic therapy in non-small cell lung cancer. BMC Med Genomics 2016;9 Suppl 1:28.
PUBMED | CROSSREF

35. Yu JE, Han SY, Wolfson B, Zhou Q. The role of endothelial lipase in lipid metabolism, inflammation, and cancer. Histol Histopathol 2018;33:1-10.
PUBMED

36. Lo PK, Yao Y, Lee JS, Zhang Y, Huang W, Kane MA, et al. LIPG signaling promotes tumor initiation and metastasis of human basal-like triple-negative breast cancer. eLife 2018;7:e31334.
PUBMED | CROSSREF